Spatial Resolution of the Heavy Ion Beam Probe on LHD

T. IDO, A. SHIMIZU, M. NISHIURA, Y. HAMADA, S. KATO, A. NISHIZAWA[1)], H. NAKANO

National Institute for Fusion Science, Oroshi-cho, Toki-shi, Gifu, 509-5292, Japan

[1)]*Tono Geoscience Center, Japan Atomic Energy Agency, Toki, Gifu, Japan*

(Received 7 December 2006 / Accepted 12 March 2007)

The sizes of sample volumes, which determine the spatial resolution, are estimated by trajectory calculation for the heavy ion beam probe on LHD. The beam width, the divergence, and the beam energy difference are taken into account. From the points of view of the spatial resolution and the signal intensity, parallel beam is suitable for the injection beam. The size of the sample volume by the parallel beam with 10mm diameter is 42 mm. It is sufficient to measure the potential profile in the internal transport barrier in the LHD plasma. Taking into account the spatial profile of the beam, the spatial resolution will be better than 42 mm.

Keywords: heavy ion beam probe, HIBP, spatial resolution, sample volume

DOI: 10.1585/pfr.2.S1100

1. Introduction

Radial electric field is a key parameter to determine the confinement of magnetically confined fusion plasmas. Heavy ion beam probe (HIBP) [1] is a unique tool to measure the electrostatic potential and density fluctuation directly and simultaneously in high temperature plasmas. A HIBP has been installed on the Large Helical Device (LHD) in order to study the transport phenomena in plasmas [2].

In the HIBP, singly charged positive ions, referred as the primary beam, are injected into plasma. They are ionized by collision with the plasma on their trajectory. Some of them become doubly charged ions, referred as the secondary beam, in the ionization and depart from the plasma. In the process, the total energy of the injected ions increases by the electrostatic potential energy at the ionization position. The secondary beams are produced along the primary beam trajectory, but the ionization position of the detected secondary beam can be estimated by the trajectory calculation because the injection- and detection-positions and the beam energy are known. Thus, we can measure the electrostatic potential at the ionization position through the energy analysis of the secondary beam.

In the experimental condition, the beam has a finite width and the detector also has a finite area, so the detected secondary beam comes from a finite volume. Thus, the observed region has a finite volume, which is referred as a sample volume. The size of the sample volume determines the spatial resolution of the HIBP. Therefore, the estimation and the optimization of the sample volume are important for the high spatial resolution, and they are estimated for previous HIBPs [3, 4].

In this article, we estimate the sample volumes of the LHD-HIBP with trajectory calculation. In the section 2, we estimate the sample volume which is formed by a beam with designed conditions. In the section 3, the beam width, divergence, and energy difference are taken into account, and the effects on the sample volumes are estimated. In the section 4, the spatial resolution is evaluated and the guide line for the optimization is discussed.

author's e-mail: ido@LHD.nifs.ac.jp

2. Sample Volumes by a Beam with Designed Properties

In the case that a probing beam is injected from the designed point with mono-energy and no divergence, the sample volume becomes a line segment on the primary beam trajectory. The length is determined by the slit opening (1 mm × 30 mm) in front of the energy analyzer. The length of the sample volumes are shown in Fig. 1, where the horizontal axis indicates the position of the sample volumes. The size of the sample volumes is almost constant (~0.55 mm), and it means that the spatial resolution does not depend on the position of the sample volume signifi-

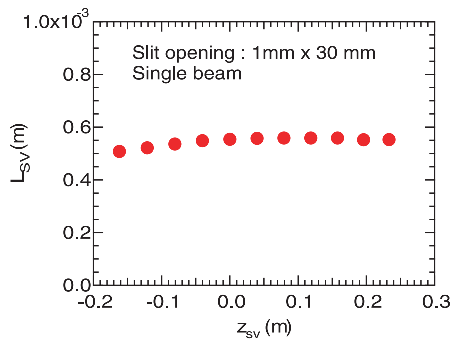

Fig. 1 Length of sample volumes when the designed beam is injected. The horizontal axis is the position of the sample volume.

cantly. In the latter sections, the size of the sample volume is calculated when the sample volume is located near the plasma center ($z_{sv} = 0$).

3. Expansion of the Sample Volumes by the Beam Width, the Divergence, and the Energy Difference

In this section, the beam width, the divergence of the beam, and the energy difference are taken into account to estimate the sample volume.

A sample volume spreads in three-dimensional space as shown in Fig. 2, so its size should be expressed with the volume. In this article, however, we ignore the toroidal dimension and estimate the maximum length in residual dimensions (the major-radius and the vertical directions) so as to estimate the spatial resolution on a poloidal plane. The length is expressed by L_{sv} in this paper.

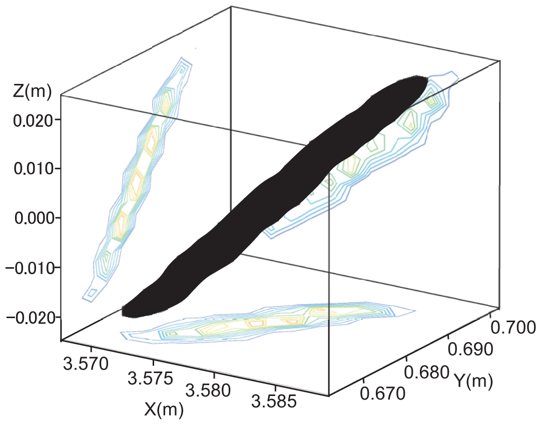

Fig. 2 A sample volume, assuming the beam with the diameter of 10 mm is injected into the designed direction. X-, Y-, and Z-axes are the major radius, toroidal displacement, and vertical axis, respectively, as shown in Fig. 3. In the calculation, the beam with the diameter of 10 mm is divided to 1290 pencil beams, and the black area shows the bunch of the ionization positions of the detectable secondary beams and it is the sample volume. Each contour indicates the distribution of the number of the ionization positions projected on each plane.

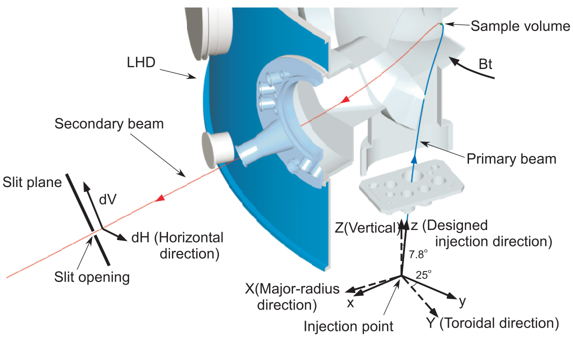

Fig. 3 Typical beam trajectory and the coordinate.

The X, Y, Z coordinate is a rectangular coordinate system, where the X axis parallel to the major radius, the Y axis is parallel to the toroidal direction at the injection point. The x, y, z coordinate system is a transformed coordinate, where the X, Y, Z coordinate is rotated 25 degree about Z axis and 7.8 degree about the transformed Y axis (y axis). The z axis is along the designed injection direction, as shown in Fig. 3.

3.1 Beam width (Δw)

Figure 4 (a) shows the intersection between the secondary beam trajectories and the slit plane, which is a plane including the slit opening and perpendicular to the designed beam line as shown in Fig. 3. Since the secondary beams are produced on the primary beam trajectory and

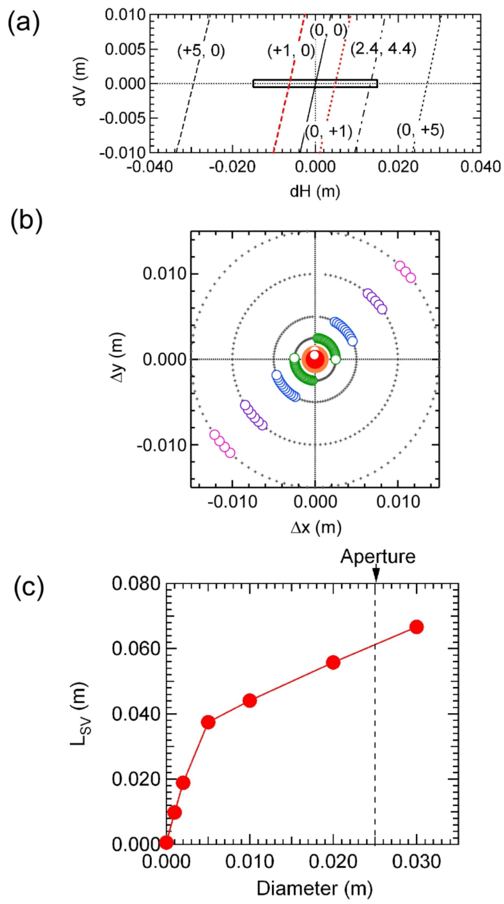

Fig. 4 Intersection between the secondary beam trajectories and the slit plane. dV and dH indicate the distances from the center on the slit in the vertical and horizontal directions, respectively. The numbers in the figure indicate the injection condition as (Δx, Δy). (b) Initial injection conditions with which the secondary beams can be detected by the detector. The conditions marked by + indicate the initial conditions which are used in the calculation. The conditions marked by circles indicate that the secondary beam with the initial conditions can be detected. (c) beam-width dependence of L_{sv}.

they become a sort of sheet beam, the intersection becomes a curved line. The origin indicates the center of the slit. It indicates that the beams with the diameter of 2 mm or larger starts to come out of the detector. However, the displacement of the intersection due to Δx is opposite to that by Δy, so the displacement can be compensate with the appropriate combination of Δx and Δy. Figure 4 (b) shows the calculated initial conditions. The secondary beam can be detected when the primary beam is injected with the initial condition marked by the circles.

The beam-width dependence of the size of the sample volume (L_{sv}) is shown in Fig. 4 (c). The diameter of the aperture in the injection-side beam line is 25 mm, so the L_{sv} can be 63 mm at most.

3.2 Divergence

Figure 5 (a) shows the change in the intersection between the secondary beam trajectories and the slit plane when the divergence is changed. The displacement of the intersection due to the divergence in the x-direction

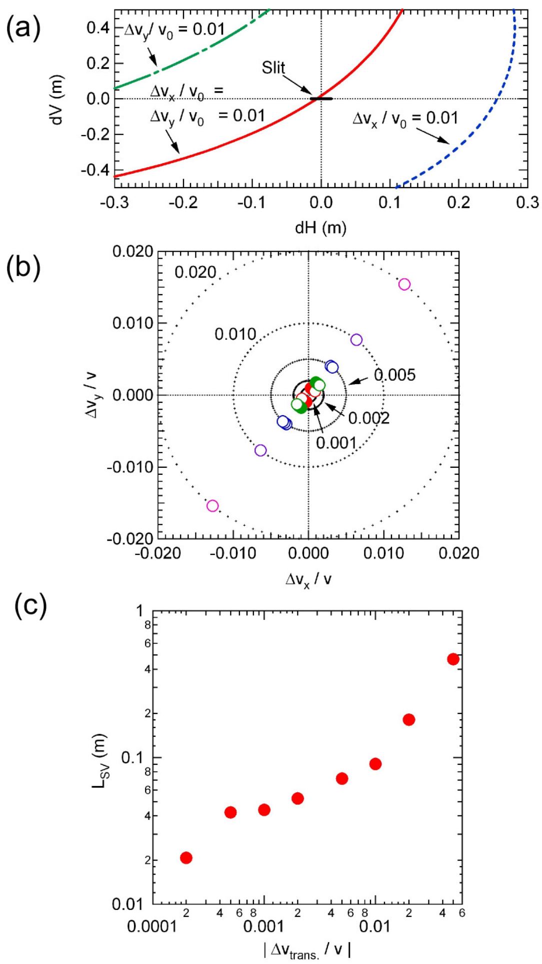

Fig. 5 (a)Intersection between the secondary beam trajectories and the slit plane. (b) Injection conditions. (c) Divergence dependence of Lsv. The horizontal axis is the divergence and $\Delta v_{trans} = \sqrt{\Delta v_x^2 + \Delta v_y^2}$.

($\Delta v_x / v_0$) is opposite to that due to the divergence in the y-direction ($\Delta v_y / v_0$). The relation is similar to that of displacement due to the beam width.

The calculated injection conditions are shown in Fig. 5 (b). The initial conditions marked with circles indicate that the beam with the initial conditions can be detected. Compared with Fig. 4 (b), they are distributed in quite narrow region in the divergence space.

The divergence dependence of L_{sv} is shown in Fig. 5 (c). The diverging beam is injected with $\Delta v_{trans}/v_0$, where $\Delta v_{trans}^2 = \Delta v_x^2 + \Delta v_y^2$. The divergence is limited to 0.05 by the sweeper geometrically. The size of the sample volume could be about 0.5 m if the divergence is not appropriate.

3.3 Beam energy

The finite energy distribution of the probing beam causes the expansion of the sample volume because the beam with the different energy traces different trajectory.

In the LHD-HIBP system, possible sources of the energy difference are sputter-type negative ion source and a tandem accelerator.

The energy spread due to the negative ions source has been measured and it is about 8 eV [5]. In the tandem accelerator, a gas cell is used to strip electrons from the injected negative ions. The energy spread is predicted to be 20 electron-volts or less [6]. Thus, 20 eV is the minimum energy spread of the probing beam.

In addition to that, if the gas pressure in the gas cell is not suitable and the pressure in the accelerator tube is not negligible, the charge-stripping process occurs in the accelerator tube. As the results, the beam with lower energy is produced. On the other hands, we use a cylindrical deflector in order to deflect the beam at 90 degrees towards the LHD, and it also works as an energy filter. The radius of the deflector (R) is 4.8 m and the gap of the electrodes (ΔR) are 30 mm, so the energy difference (ΔK) of the beam which can pass through the deflector is estimated as $\Delta K/K_0 \sim \Delta R/R \sim 6.25 \times 10^{-3}$, and $\Delta K \sim 37.5$ (keV) for the beam energy (K_0) of 6 MeV. Thus, the maximum energy difference for the 6 MeV beam is 37.5 kV.

Figure 6 (a) shows the intersection between the secondary beam trajectories and the slit plane. It indicates that the probing beams with the energy difference of 22 keV or more is not detected and they do not contribute to form the sample volumes.

The energy-difference dependence of L_{sv} is shown in Fig. 6 (b), where the beam energy is from $K_0 - \Delta K_0$ to K_0. It indicates that the size of the sample volume increases linearly with $|\Delta K_0|$ in the case $|\Delta K_0| \leq 20$ keV. In the case that $|\Delta K_0| > 20$ keV, the size of the sample volumes is constant because the beam with $|\Delta K_0| > 20$ keV is not detected as shown in Fig. 6 (a).

The expansion of the sample volume due to the energy difference is 12 mm at most. On the other hand, if the

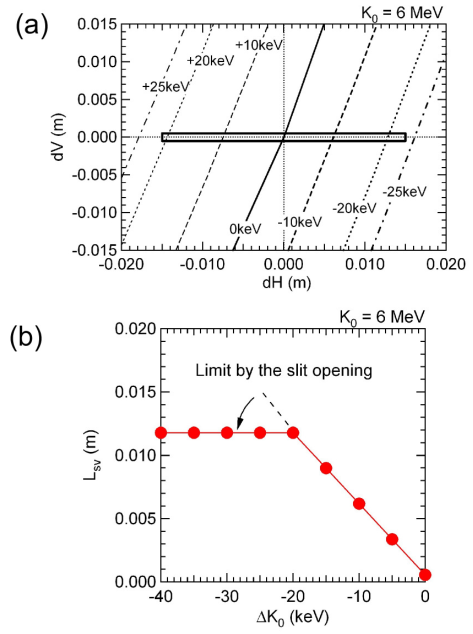

Fig. 6 (a) Intersection between the secondary beam trajectories and the slit plane. (b) Energy-difference dependence of L_{sv}. The injected beam energy is from $K_0 - \varDelta K_0$ to K_0.

charge stripping in the accelerator tube can be negligible, the expansion of L_{sv} is negligible size. Thus, the minimization of the pressure in the accelerator tube is important.

4. Discussion

We discuss the guide line to optimize the spatial resolution.

In the experiment, the beam width and the divergence can be controlled by doublet-quadrupole lenses in the injection-side beam line. Judging from Fig. 4 (c) and Fig. 5 (c), the divergence expands the sample volume more effectively than the beam width does. For example, a divergence of 0.01, that is possible value in the experiment, causes L_{sv} of 100 mm, though the maximum beam width which is limited to 25 mm by an injection-side aperture causes L_{sv} of 63 mm. In addition to that, the detectable initial-condition region in the divergence space (Fig. 5 (b)) is narrower than that in the beam width space (Fig. 4 (b)). From the view point of the secondary beam intensity, the divergence should be as small as possible. Thus, a parallel beam, $\varDelta v_{trans}/v_0 = 0$, is preferred for measurement with the better spatial resolution.

The parallel beam with the diameter of 10 mm can be injected in present experiments, and the size of the sample volume is 42 mm as shown in Fig. 4 (c). It is enough small to observe the potential profile in the electron internal transport barrier [7–9] in the LHD plasmas because the characteristic scale length is a few hundred mili-meters. However, assuming turbulence satisfies $k\rho_i \sim 1$, where k is the wave number of the turbulence and ρ_i is the ion's Larmor radius, the size of the sample volume is larger than the wave length of the turbulence (~ a few ten mili-meters).

One of methods to reduce the sample volume is to narrow the slit opening. As shown in Fig. 4-6 (a), the horizontal width of the slit determines the size of the sample volume. In the case that the slit opening is 1 mm × 15 mm, which is a half of the present slit width, the size of the sample volume becomes 28 mm. It is comparable to the turbulence with $k\rho_i \sim 1$.

Actually, the estimated size of the sample volume is the length of the largest dimension, but most of the secondary beams come from smaller region of the sample volume as shown by the contours in Fig. 2. In addition to that, since the probing beam has a spatial profile peaked at the center of the beam, the information from the central region of the sample volume becomes dominant. Thus, the effective spatial resolution is smaller than the above estimated size of the sample volume. The analysis including the beam profile is necessary to assess the ability of the turbulence measurement.

Acknowledgements

We thank Prof. T. Watanabe for the accurate magnetic field data. We are also grateful to Prof. O. Motojima, Prof. S. Sudo and the LHD Experimental group for their continuous support and the fruitful discussion.

This work was supported by MEXT Japan under Grants-in-Aid for Scientific Research (nos. 16760674 and 18760640) and the NIFS budget (nos. NIFS05ULBB505, 507, and 508).

[1] R.L. Hickok, Rev. Sci. Instrum. **38**, 142 (1967).
[2] T. Ido *et al.*, Rev. Sci. Instrum. **77**, 10F523 (2006).
[3] T.P. Crowley *et al.*, Fusion Engineering and Design **34-35**, 653 (1997).
[4] T. Ido *et al.*, Plasma Phys. Control. Fusion **41**, 1013 (1999).
[5] A. Taniike, M. Sasao, A. Fujisawa, H. Iguchi, Y. Hamada, J. Fujita, M. Wada, Y. Mori, IEEE Trans. Plasma Sci. **22**, 430 (1994).
[6] A. Taniike, M. Sasao, J. Fujita, Y. Hamada, M. Wada, Fusion Engineering and Design **34-35**, 675 (1997).
[7] T. Shimozuma *et al.*, Plasma Phys. Control. Fusion **45**, 1183 (2003).
[8] Y. Takeiri *et al.*, Phys. Plasmas **10**, 1788 (2003).
[9] K. Ida *et al.*, Phys. Rev. Lett. **91**, 085003 (2003).